The Journal of Chemical Physics

Hysteresis curves reveal the microscopic origin of cooperative CO_2 adsorption in diamine-appended metal–organic frameworks

Cite as: J. Chem. Phys. **154**, 214704 (2021); https://doi.org/10.1063/5.0054794
Submitted: 22 April 2021 . Accepted: 01 May 2021 . Published Online: 01 June 2021

John R. Edison, Rebecca L. Siegelman, Zdeněk Preisler, Joyjit Kundu, Jeffrey R. Long, and Stephen Whitelam

View Online Export Citation CrossMark

ARTICLES YOU MAY BE INTERESTED IN

Deep learning combined with IAST to screen thermodynamically feasible MOFs for adsorption-based separation of multiple binary mixtures
The Journal of Chemical Physics **154**, 234102 (2021); https://doi.org/10.1063/5.0048736

Molecular dynamics study of water confined in MIL-101 metal-organic frameworks
The Journal of Chemical Physics **154**, 144503 (2021); https://doi.org/10.1063/5.0040909

In silico design of a new Zn-triazole based metal-organic framework for CO_2 and H_2O adsorption
The Journal of Chemical Physics **154**, 024303 (2021); https://doi.org/10.1063/5.0037594

Challenge us.
What are your needs for periodic signal detection?
Watch
Zurich Instruments

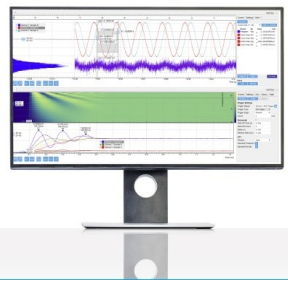

© 2021 Author(s).

The Journal of Chemical Physics ARTICLE scitation.org/journal/jcp

Hysteresis curves reveal the microscopic origin of cooperative CO_2 adsorption in diamine-appended metal–organic frameworks

Cite as: J. Chem. Phys. 154, 214704 (2021); doi: 10.1063/5.0054794
Submitted: 22 April 2021 • Accepted: 1 May 2021 •
Published Online: 1 June 2021

View Online Export Citation CrossMark

John R. Edison,[1,2,a] Rebecca L. Siegelman,[3,4] Zdeněk Preisler,[1] Joyjit Kundu,[1,5,6,a] Jeffrey R. Long,[3,4,7] and Stephen Whitelam[1,a]

AFFILIATIONS

[1] Molecular Foundry, Lawrence Berkeley National Laboratory, 1 Cyclotron Road, Berkeley, California 94720, USA
[2] Department of Chemical and Biomolecular Engineering, Johns Hopkins University, Baltimore, Maryland 21218, USA
[3] Department of Chemistry, University of California, Berkeley, California 94720, USA
[4] Materials Sciences Division, Lawrence Berkeley National Laboratory, Berkeley, California 94720, USA
[5] Department of Chemistry, Duke University, Durham, North Carolina 27708, USA
[6] Department of Physics, Indian Institute of Technology Hyderabad, Kandi, Sangareddy, TN 502285, India
[7] Department of Chemical and Biomolecular Engineering, University of California, Berkeley, California 94720, USA

[a] **Authors to whom correspondence should be addressed:** dayakaran@jhu.edu; swhitelam@lbl.gov; and joyjitkundu032@gmail.com

ABSTRACT

Diamine-appended metal–organic frameworks (MOFs) of the form $Mg_2(dobpdc)(diamine)_2$ adsorb CO_2 in a cooperative fashion, exhibiting an abrupt change in CO_2 occupancy with pressure or temperature. This change is accompanied by hysteresis. While hysteresis is suggestive of a first-order phase transition, we show that hysteretic temperature-occupancy curves associated with this material are qualitatively unlike the curves seen in the presence of a phase transition; they are instead consistent with CO_2 chain polymerization, within one-dimensional channels in the MOF, in the absence of a phase transition. Our simulations of a microscopic model reproduce this dynamics, providing a physical understanding of cooperative adsorption in this industrially important class of materials.

Published under license by AIP Publishing. https://doi.org/10.1063/5.0054794

I. INTRODUCTION

Metal–organic frameworks (MOFs) are porous, crystalline materials with large internal surface areas and have been studied extensively as adsorbents for gas storage and separations.[1–3] The recently developed MOFs $Mg_2(dobpdc)(diamine)_2$ are particularly promising in this regard because they exhibit cooperative adsorption in which a conveniently small change in pressure or temperature results in an abrupt change in the quantity of CO_2 adsorbed by the framework.[4–6] In a majority of the cases, cooperative adsorption results from a guest-induced phase transition or dynamic rearrangement of the MOF structure or a phase transition of the adsorbed gas.[7–13] However, gas adsorption in the diamine-appended MOFs proceeds through the formation of one-dimensional structures without abrupt changes in the framework.[5] As described in Ref. 5, proton transfer and nucleophilic attack of N on a CO_2 molecule forms an ammonium carbamate species and induces a chain reaction that leads to the cooperative insertion of CO_2 into the metal–amine bonds. The result is a chain of ammonium carbamate formed along the MOF pore axis. The one-dimensional nature of this process, and the physics of one-dimensional phenomena, suggests that cooperative gas uptake in diamine-appended $Mg_2(dobpdc)$ materials occurs in the *absence* of a phase transition.[14] Clarifying this issue is important in order to establish a microscopic understanding of cooperative gas uptake.

In previous work,[15] we used a statistical mechanical model of CO_2 adsorption within the MOFs $Mg_2(dobpdc)(diamine)_2$ to show that the process of ammonium carbamate chain formation is

Published under license by AIP Publishing

associated with cooperative thermodynamics consistent with the experimental data. That work provided evidence for the claim that a phase transition does not need to occur in this class of materials in order to observe cooperative binding. In this paper, we study the *dynamics* of cooperative adsorption in the representative diamine-appended MOF e-2–Mg_2(dobpdc) (e-2 = *N*-ethylethylenediamine). We find that dynamics also indicates that cooperative adsorption occurs in the absence of a phase transition. In particular, the hysteresis seen in temperature-occupancy curves resembles the hysteresis produced by slow diffusive dynamics and not the hysteresis resulting from nucleation during a first-order phase transition.

Hysteresis, a memory of the prior state of the system, is indeed normally associated with a first-order phase transition, which involves a discontinuous change in an order parameter (e.g., gas occupancy) with a control parameter (e.g., temperature). In that scenario, hysteresis arises from the slow dynamics of nucleation, i.e., the potentially long time required for thermal fluctuations to produce a nucleus of the stable phase (the time during which the system remains "stuck" in its initial state).[16,17] However, hysteresis results more generally whenever an order parameter of the system changes less rapidly than its control parameter and so can also arise in the absence of a phase transition. For instance, force–extension curves for DNA stretching display hysteresis associated with the slow detachment of the two strands of the helix.[18–21] Here, we present the experimental and simulation data showing that the nature of hysteresis in temperature-occupancy data for CO_2 in e-2–Mg_2(dobpdc) is consistent with CO_2 polymerization in the absence of an underlying phase transition. In particular, we compare the computational and experimental observations based on scanning curves at various rates of temperature change. Our work provides a link between microscopic models of gas adsorption and experimental data and provides fundamental understanding of a phenomenon of experimental and industrial importance.

This paper is organized as follows: In Sec. II, we describe the experimental setup used to measure gas-adsorption and scanning curves in the diamine-appended MOF e-2–Mg_2(dobpdc) (e-2 = *N*-ethylethylenediamine). In Sec. III, we describe our statistical mechanical model of the same and summarize the simulation protocols and analytic methods we use to study it. In Sec. IV, we present a comparison of gas-adsorption curves in experiment and simulation and compare these results to the generic behavior expected in the presence and absence of a phase transition; our data are consistent with the latter scenario. We conclude in Sec. V.

II. EXPERIMENTAL METHODS

A. Synthesis of e-2–Mg_2(dobpdc)

The metal–organic framework Mg_2(dobpdc) was synthesized, washed, and characterized following a previously reported procedure.[22] Post-synthetic functionalization to prepare the diamine-appended framework e-2–Mg_2(dobpdc) was performed as reported previously.[22] The diamine loading was determined following the literature procedure[22] by collecting ^{1}H nuclear magnetic resonance (NMR) spectra of material digested with DCl (35 wt. % in D_2O) in dimethyl sulfoxide (DMSO)-d_6. Spectra were collected on a Bruker AMX 300 MHz NMR spectrometer and referenced to residual DMSO (δ 2.50 ppm). The diamine loading of as-synthesized e-2–Mg_2(dobpdc) was found to be 125%, as determined from the ratio of the diamine to ligand peak integrals. A representative diamine loading of 98% was determined following the isobar collection. All adsorption data were collected on individual aliquots of a single sample within one week of preparation.

All synthetic manipulations were carried out under air. All solvents and the diamine e-2 (*N*-ethylethylenediamine) were purchased from commercial suppliers and used without further purification. The ligand 4,4′-dihydroxy-(1,1′-biphenyl)-3,3′-dicarboxylic acid (H_4dobpdc) was obtained from Hangzhou Trylead Chemical Technology Co., Ltd.

B. Thermogravimetric analysis of gas uptake

Ultra-high purity gases (>99.998%) were used for all adsorption experiments. Adsorption and desorption isobars were collected using a TGA Q5000 thermogravimetric analyzer. A flow rate of 10 ml/min was used for all gases, and masses were uncorrected for buoyancy effects. Samples were activated at 120 °C for 20 min under pure N_2 before isobar collection. Isobars were measured under pure CO_2 at atmospheric pressure using a temperature ramp rate of 1 °C/min. Results are presented in Sec. IV.

III. MODEL AND COMPUTER SIMULATIONS

A. Statistical mechanical model of gas uptake in e-2–Mg_2(dobpdc)

We used a one-dimensional lattice model to study the adsorption of CO_2 in amine-appended MOFs, a detailed justification of which is presented in Ref. 15. Figure 1 shows a schematic of the model. A lattice site can be unoccupied (state U) or occupied by a gas molecule. An adsorbed gas molecule can bind individually (state S) to a site or it can be part of a polymerized chain by forming active

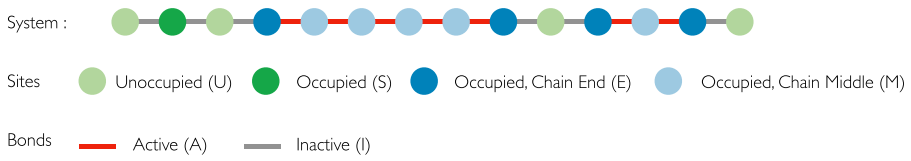

FIG. 1. (a) Schematic of our statistical mechanical model of a diamine-appended MOF (see Ref. 15 for additional details). Each site of the lattice can be unoccupied (U) or occupied by individual CO_2 molecules (S) or CO_2 molecules at the end (E) or middle (M) of polymerized chains. Chains are held together by active (A) bonds, while inactive (I) bonds connect all other sites. The rates for changes of these states are given in Table I.

Published under license by AIP Publishing

(A) links with one or two neighboring gas molecules. The states E (end) and M (middle) distinguish between gas molecules that are at the ends and middle of a chain. As in Ref. 15, we set the binding constants of the gas molecules in the occupied S, M, and E states (see Fig. 1) to $E_S = -\epsilon$, $E_E = -2.592\epsilon$, and $E_M = -3.24\epsilon$. The energy scale $\epsilon = 22.6$ kJ/mol is the binding energy of a single CO_2 molecule within the framework. These energetic parameters are appropriate for the metal Mg and were obtained using vdW-corrected quantum mechanical density-functional theory calculations. For details of the calculation, see Secs. S1 and S2 of the supplemental material of Ref. 15.

This model reproduces the cooperative adsorption of CO_2 within the diamine-appended MOFs. Our prior analysis of the model[15] indicates that an abrupt (but finite) increase in the mean length of polymerized CO_2 chains with temperature gives rise to a step-like uptake curve in the absence of a phase transition. The associated adsorption curves agree qualitatively and semi-quantitatively with the experimental data.[15]

B. Simulation protocol

We used a Kinetic Monte Carlo (KMC) scheme to simulate the dynamics of the lattice model. A KMC scheme involves a set of possible events and a rate r_i for each event i. Events occur randomly, in proportion to their rates, and time advances by a random amount that is drawn from an exponential distribution with the parameter equal to the rate of the enacted event.[23]

Table I lists the events and rates we consider, which include the binding and unbinding of CO_2 molecules and the formation and breaking of bonds between them. All events are modeled as barrier-hopping processes. In Fig. 2, we show a schematic of two such events. The constants ω_0 and ϵ set the time- and energy scales of the system. Recall that the energy scale $\epsilon = 22.6$ kJ/mol is the binding energy of a single CO_2 molecule within the framework; the timescale ω_0 is determined as described below. We set the barrier height for the site transition to $E_{bs} = \epsilon/2$ and the barrier height for all bond transitions to $E_{bb} = \epsilon$, and verified via numerical simulations that small variations in these choices do not affect the conclusions of our work.

TABLE I. Events and rates for the model of Fig. 1. We allow processes involving single sites (first two lines) or pairs of neighboring sites and their adjoining bond (subsequent lines). The energetic parameters are $E_S = -\epsilon$, $E_E = -2.592\epsilon$, $E_M = -3.24\epsilon$, $\beta\mu = -13.5$, $E_{bs} = 0.5\epsilon$, and $E_{bb} = \epsilon$. Here, $\beta = \epsilon/(k_B T)$. The parameter $\epsilon = 22.6$ kJ/mol is the binding energy of a single CO_2 molecule in the MOF, obtained using quantum mechanical density-functional theory.[15]

Event	Rate
U → S	$\omega_0 \exp[\beta(\mu - E_{bs})]$
S → U	$\omega_0 \exp[\beta(E_S - E_{bs})]$
SS[I] → EE[A]	$\omega_0 \exp[-\beta E_{bb}]$
EE[A] → SS[I]	$\omega_0 \exp[\beta(2(E_E - E_S) - E_{bb})]$
EE[I] → MM[A]	$\omega_0 \exp[-\beta E_{bb}]$
MM[A] → EE[I]	$\omega_0 \exp[\beta(2(E_M - E_E) - E_{bb})]$
SE[I] → EM[A]	$\omega_0 \exp[-\beta E_{bb}]$
EM[A] → SE[I]	$\omega_0 \exp[\beta(E_M - E_S - E_{bb})]$
ES[I] → ME[A]	$\omega_0 \exp[-\beta E_{bb}]$
ME[A] → ES[I]	$\omega_0 \exp[\beta(E_M - E_S - E_{bb})]$

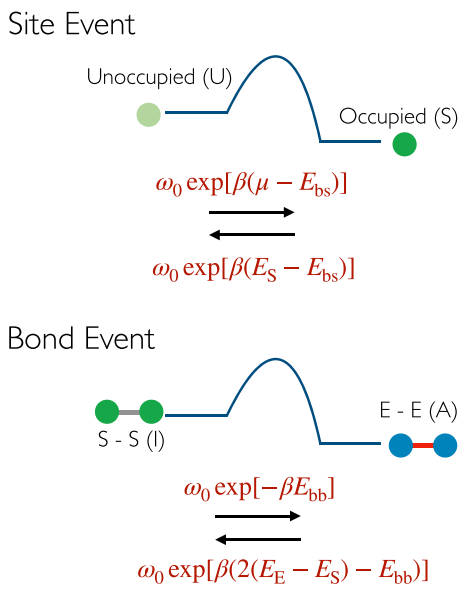

FIG. 2. A schematic representation of site-changing- and bond-changing events in the model of Fig. 1. The forward and backward rates for these events are shown above and below the arrows.

To run gas-uptake KMC simulations resembling the experimental protocol, we proceed as follows: We set the activity of the system to be $\beta\mu = -13.5$. We begin with an empty lattice of size $N = 4096$. The initial temperature is set to T_0. We evolve the system for a fixed observation time $t_{obs} = 10^8$ and measure the gas occupancy. We then make a small fixed decrement in the temperature and again compute the uptake after a fixed observation time t_{obs}. These two steps are repeated until the system reaches a final temperature T_f. We then reverse the process until the system reaches the initial temperature T_0. The curves reported in Fig. 4 are an average of 120 statistically independent runs.

In Ref. 15, we showed that the model was qualitatively accurate with respect to thermodynamic quantities: the model captures the correct energy and temperature scales of the experimental system, but small uncertainties in calculated binding energies resulted in uncertainties in calculated gas-uptake curves. In this paper, we performed simulations at a higher temperature range (540–750 K) than the experiments (≈380–420 K). In the experimental temperature range, the observation time required to obtain reliable statistics is beyond our computational capability. Results of simulations and experiments can therefore be compared only qualitatively. For this reason, we report simulation results in terms of reduced temperatures. We know from exact analysis that the model's gas-uptake mechanism is the same in the regime probed by simulations and the experimental regime, and running simulations at artificially high temperatures should be seen as a device to obtain results on manageable timescales.

Published under license by AIP Publishing

C. Measurement of relaxation rate

We measured the relaxation rate k of the system at a thermodynamic state $(\beta\mu, T)$ as follows: The system is initially equilibrated at a certain value of temperature T_0 and activity $(\beta\mu)$ or pressure and has a CO_2 occupancy ρ_0. We then make an abrupt change in temperature. Following this change, we measured the CO_2 occupancy $\rho(t)$, averaged over 120 trajectories, until equilibrium is achieved. We compared the final density ρ_f measured in simulations with the exact analytical transfer-matrix calculations of our model[15] to ensure that the system has equilibrated. We fit $\bar{\rho}(t) = (\rho_f - \rho(t))/(\rho_f - \rho_0)$ to an exponential form e^{-kt}, thus obtaining k. Values obtained in this way are shown in Fig. 3. We determined the basic time scale of the system, $\omega_0 = 210\ s^{-1}$, by equating the relaxation rate measured in experiments (upon an abrupt pressure change) to the relaxation rate of our model k.

D. Analytic calculation of the model's free energy

To understand the origin of hysteresis in the model, it is convenient to calculate the curvature of the model's free-energy landscape. The grand partition function of the model is

$$\mathcal{Z} = \sum_{\{n_S, n_M, n_E\}} K_S^{n_S} K_E^{n_E} K_M^{n_M} \Gamma(n_S, n_M, n_E), \tag{1}$$

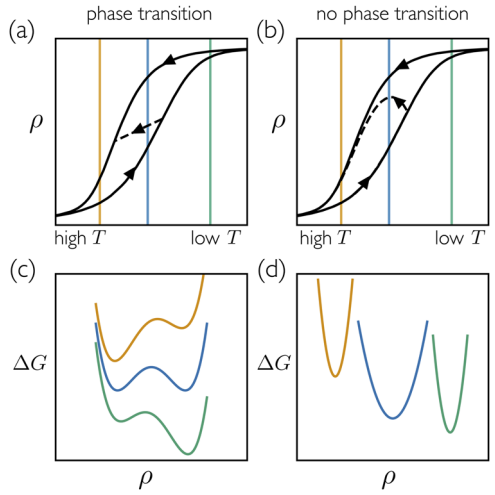

FIG. 3. Schematic adsorption–desorption in the presence and absence of a phase transition. (a) Generic adsorption (up arrow) and desorption (down arrow) curves, in an occupancy ρ vs temperature T representation, in the presence of a first-order phase transition. Panel (c) shows the associated free-energy (ΔG) profiles. The black dashed line in panel (a) shows an "early-stop" desorption scanning curve initiated from partway up the adsorption curve: this desorption curve decreases monotonically as we move left because the large timescale required to access the stable state prevents the curve from moving upward toward the point corresponding to the global free-energy minimum. (b) By contrast, desorption curves in the absence of a first-order phase transition are non-monotonic because the system can evolve toward the global free-energy minimum on the timescale of observation. Panel (d) shows the associated free-energy profiles. The colored vertical lines in panels (a) and (b) correspond to the similarly colored profiles in panels (c) and (d), respectively.

where

$$\Gamma(n_S, n_M, n_E) = \frac{(N - n_M - n_E/2)!}{(N - n_S - n_M - n_E)!(n_E/2)!n_1!} \times \frac{(n_E/2 + n_M - 1)!}{(n_E/2 - 1)!n_M!} \tag{2}$$

is the number of ways of arranging n_S single molecules, n_M internal chain molecules, and n_E chain end-points on a one-dimensional lattice of N sites. The quantity K_α, with $\alpha \in \{S, M, S\}$, is the statistical weight of a CO_2 molecule in conformation α. The free energy in the thermodynamic limit is

$$\begin{aligned} f(x_S, x_M, x_E) = &-\left(1 - x_M - \frac{x_E}{2}\right)\ln\left(1 - x_M - \frac{x_E}{2}\right) \\ &- \left(x_M + \frac{x_E}{2}\right)\ln\left(x_M + \frac{x_E}{2}\right) + x_S \ln x_S \\ &+ x_M \ln x_M + x_E \ln \frac{x_E}{2} \\ &+ (1 - x_S - x_M - x_E)\ln(1 - x_S - x_M - x_E), \end{aligned} \tag{3}$$

where x_α, with $\alpha \in \{S, M, E\}$, is the fraction of CO_2 molecules in conformation α.

The Hessian H is a 3×3 matrix built from the three variables x_S, x_M, and x_E, with matrix elements

$$H_{\alpha\beta} = \left.\frac{\delta^2 f(x_S, x_M, x_E)}{\delta x_\alpha \delta x_\beta}\right|_{\min} \tag{4}$$

evaluated at the free-energy minimum.

At a given pressure (the statistical weight K_α is proportional to the pressure), we evaluated $H_{\alpha\beta}$ at the equilibrium values of x_S, x_M, and x_E and calculated the three eigenvalues. We find that the smallest eigenvalue (called λ in Fig. 6), which corresponds to the slowest mode of relaxation, has a minimum near the inflection point of the isobar. The quantity λ is a measure of the curvature of the free-energy landscape in terms of the coordinates $\{x_S, x_M, x_E\}$.

IV. RESULTS

A. Qualitative overview of hysteresis in gas-uptake data

Before comparing experimental and simulation data, we summarize in Figs. 3(a) and 3(c) the canonical case of hysteresis accompanying a first-order phase transition. In Fig. 3(a), we show typical adsorption–desorption curves[24] for an ordered porous material with a narrow pore-size distribution, as a function of temperature T, for the case in which the adsorbate or framework undergoes a first-order phase transition (or a "rounded" transition if the system is of finite size[25]). In Fig. 3(c), we show the accompanying free-energy landscape for a single pore.[16,17]

The origin of hysteresis in this scenario is the slow dynamics of nucleation: we must wait for a thermal fluctuation to generate a nucleus of the stable phase. Near phase coexistence, the nucleation time is large and can therefore exceed the experimental observation time. However, the system retains the ability to relax to the local or metastable equilibrium as T is varied.[26] This separation of timescales can be identified by "early-stop" desorption scans, initiated partway up the adsorption curve. One such example is shown

Published under license by AIP Publishing

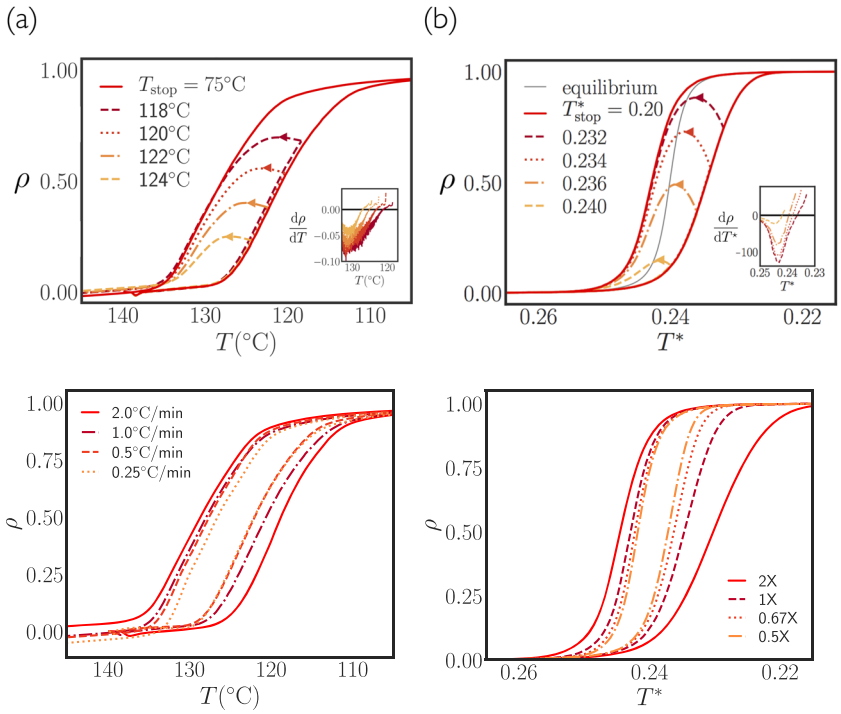

FIG. 4. Early-stop desorption scanning curves for (a) CO_2 occupancy ρ in the MOF e-2–Mg_2(dobpdc) and (b) our simulation model of the same are consistent with Fig. 3(b): the qualitative nature of hysteresis indicates the *absence* of a phase transition in this MOF. T_{stop} is the temperature at which the scanning curve is reversed. Arrows point in the direction of the scanning curve. The insets to both panels show the gradients of the scanning curves, which change sign. In panel (b), $T^* \equiv k_B T/\epsilon$, where $\epsilon = 22.6$ kJ/mol is a basic unit of energy. The basic unit of simulation time is determined in Sec. III.

FIG. 5. As Fig. 4(b), but for different rates of temperature scan. Experiment (left) and simulation (right) are qualitatively consistent: changes in the scan rate result in changes in the width of the hysteresis loops.

as a black dashed line in Fig. 3(a). As T increases (moving left in the figure), the adsorbate loading (dashed line) decreases monotonically: pores that are empty when the desorption scan begins remain so as the scan proceeds[27–31] (see Fig. 17 of Ref. 17). Materials that display adsorption hysteresis due to an underlying structural transition show similar behavior.[12]

By contrast, we expect early-stop desorption experiments in the absence of a phase transition to behave as in Fig. 3(b). The associated free-energy surface, shown in Fig. 3(d), has a single minimum under all conditions, and the system should be able to evolve in the direction of this minimum on the timescale of the experiment. For a given pressure and temperature, the MOF-gas system has a single free-energy minimum. The gray curve in Fig. 4(b) shows the equilibrium occupancy corresponding to this minimum. Near the inflection point of this curve, dynamical relaxation to the minimum is slow. In the early-stop experiments and simulations, the observation time is smaller than the system's relaxation time. Therefore, the system is out of equilibrium and is in the process of evolving toward the equilibrium occupancy curve. To the right of the inflection point, the equilibrium occupancy is higher than the system's current occupancy, and so the scanning curve points upward. To the left of the inflection point, the scanning curve points downward. The result is a non-monotonic early-stop desorption curve.

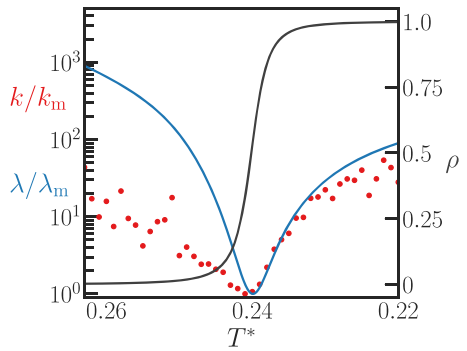

FIG. 6. The curvature of the free-energy landscape of the model, λ (blue), influences its relaxation rate k (red) along the adsorption isobar (gray). At the inflection point of the isobar, the flatness of the free-energy landscape results in slow dynamics and the hysteresis seen in Fig. 4. The parameters $k_m \approx 1.30 \times 10^{-9}\ s^{-1}$ and $\lambda_m \approx 0.267$ are reference values of k and λ, respectively (see Secs. III C and IV D).

B. Experimental data are consistent with the absence of a phase transition

In Fig. 4(a), we show the experimental adsorption and desorption curves for CO_2 in the representative diamine-appended MOF e-2–Mg_2(dobpdc); experimental details are given in Sec. II. In this figure, we also show early-stop desorption curves (dotted lines) obtained by reversing the temperature scan partway up the adsorption curve. These curves behave according to the scenario shown in Fig. 3(b): the dynamics of cooperative adsorption in this MOF are qualitatively consistent with loading that proceeds in the absence of a phase transition. Similar non-monotonic behavior of the desorption curve is predicted to occur when diffusion of gas molecules within the framework is much slower than experimental timescales;[32] however, measured diffusion rates within our system[33] rule out this alternative scenario.

Published under license by AIP Publishing

C. Simulations are consistent with experiments

In Fig. 4(b), we show analogous data obtained from dynamic simulations of our statistical mechanical model. The details of our simulation are presented in Sec. III B. The figures show that the dynamic behavior of the model is consistent with the experimental data: the simulations of Fig. 4(b) are qualitatively consistent with the experiments of Fig. 4(a) and with the mechanism summarized by Fig. 3(b). Simulation results are averaged over 120 independent trajectories; error bars are smaller than the thickness of the lines. The solid line marked "equilibrium" in Fig. 4(b) is obtained by exact transfer-matrix calculation[15] while the colored lines are obtained by dynamical simulation.

We show in Fig. 5 that varying the rates of temperature scan in experiment and simulation does not qualitatively change the scenario presented: in both cases, scanning temperature more slowly causes hysteresis loops to narrow, approaching (but not reaching) the equilibrium isobar. These changes are seen for any variation in the scan rate, further supporting the picture we are presenting. Hysteresis loops resulting from an underlying phase transition are generally reproducible because very large observation times are required to see changes in hysteresis loops resulting from the changes in the scan rate. This is clearly not the case in our system: any increases in the scan rate at a fixed observation time (or increase in observation time at fixed scan rate) visibly narrow the hysteresis loop.

D. Analysis of the model provides microscopic understanding of the origin of hysteresis

To understand the origin of the model's slow dynamics, we show in Fig. 6 the equilibrium isobar of the model (gray) together with a measure of the basic collective timescale of the system, the relaxation rate k (red; see Sec. III C). The relaxation rate peaks near the inflection point of the curve. We also show λ (blue), a measure of the curvature of the free-energy surface (see Sec. III D). Near the isobar inflection point, the system possesses a free-energy landscape that is almost flat, with no strong thermodynamic driving force for CO_2 chains to grow or shrink. As a result, the relaxation time of the system is long, giving rise to hysteresis in the representation of Fig. 4. By contrast, hysteresis in the presence of a first-order phase transition results from slow nucleation of the stable phase in a background of the metastable one.

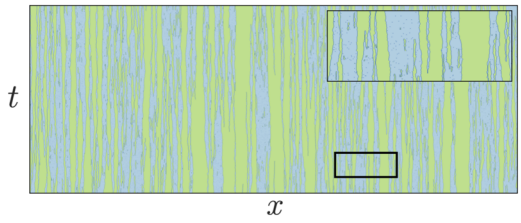

FIG. 7. Space x vs time t plot of a trajectory of our statistical mechanical model of e-2–Mg_2(dobpdc) at reduced temperature $T^* = 0.24$ (i.e., at the inflection point of the cooperative isobar; see Fig. 6). Green indicates unoccupied sites or isolated CO_2 molecules; blue indicates polymerized CO_2 molecules. The slow dynamics associated with the diffusive fluctuations of chain lengths results in the large relaxation times shown in Fig. 6 and the hysteresis shown in Fig. 4(b). The inset is an enlargement of the boxed region (see also Fig. 9).

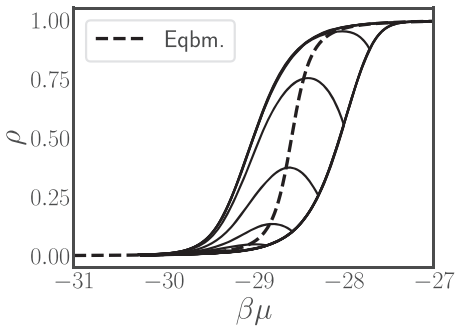

FIG. 8. As Fig. 4(b), but as a function of chemical potential $\beta\mu$ instead of temperature; the behavior is qualitatively similar. Model parameters: $E_S = 1.0$, $E_M = 2.5$, $E_t = 2.0$, and $T^* = 0.175$. The black dashed line corresponds to the equilibrium value of the occupancy obtained from exact transfer-matrix calculations.[15]

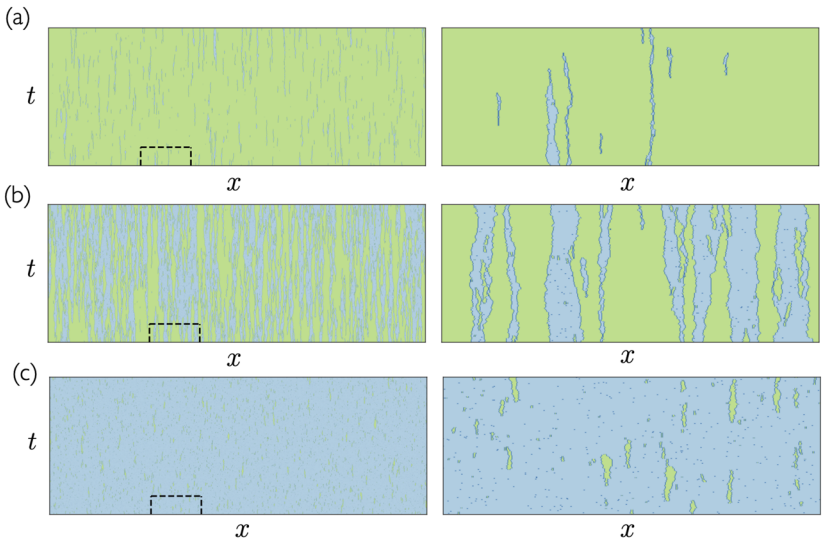

FIG. 9. Space–time plots of the model under a sudden change in chemical potential to the values (a) $\beta\mu = 29.14$, (b) $\beta\mu = -28.57$, and (c) $\beta\mu = -28.0$, which lie at and on either side of the inflection point of the curve shown in Fig. 8. Green represents unoccupied sites or isolated CO_2 molecules; blue represents polymerized CO_2 molecules. The right-hand panels are enlargements of the boxed regions.

Published under license by AIP Publishing

The microscopic dynamic consequences of the flat free-energy landscape are summarized in Fig. 7, which shows a space vs time plot from a simulation trajectory. The slow diffusive fluctuations of the polymerized CO_2 chains are apparent.

E. Hysteresis at constant temperature is similar to that at constant pressure

The hysteresis behavior described above is not particular to uptake at constant pressure. We verified that simulations of the model reveal similar hysteretic behavior in terms of uptake vs chemical potential at constant temperature (see Fig. 8). Again, scanning curves are non-monotonic. We show the space–time plots of the dynamics at constant temperature for three values of the chemical potential in Fig. 9, at and on either side of the isotherm inflection point. The behavior seen is similar to that reported in Sec. IV D and arises from the same mechanism.

V. CONCLUSIONS

Cooperative adsorption of gases is of considerable scientific and technological importance. Despite recent advances in developing materials in which cooperative adsorption occurs,[4–6] we lack a complete understanding of how the phenomenon results from the interplay of gas molecules with their host framework. Building on Ref. 15, this paper puts forward a molecular description of cooperative CO_2 adsorption in the metal–organic frameworks Mg_2(dobpdc) using the hysteresis seen in experiment as a means of distinguishing between two possible scenarios. The agreement between simulation and experiment is qualitative: as discussed in Ref. 15, small uncertainties in calculated energies result in numerical uncertainties in predictions, and at present, it is possible to achieve only semi-quantitative accuracy with experiment. Improved accuracy requires improved calculations of energetic parameters or the inclusion of additional model fitting parameters. Nonetheless, the model reveals mechanisms and trends and provides a starting point for further design of cooperative adsorbers. For instance, analysis of the model allows us to identify a range of gas–metal binding energies for which cooperative adsorption occurs and indicates qualitatively how to move the inflection point of the uptake curve to the desired values of temperature and pressure. Simulation models of gas uptake also aid in the design of protocols to achieve particular goals, e.g., to minimize dissipation,[34] a first step toward the design of energy-efficient industrial protocols.

AUTHORS' CONTRIBUTIONS

J.R.E., J.K., Z.P., and S.W. planned and carried out the simulations and R.L.S. and J.R.L. did the same for the experiments. All authors contributed to the data analysis and interpretation.

ACKNOWLEDGMENTS

The computational portion of this research was carried out as part of a user project at the Molecular Foundry at Lawrence Berkeley National Laboratory (LBNL), supported by the Office of Science, Office of Basic Energy Sciences, of the U.S. Department of Energy under Contract No. DE-AC02-05CH11231. The experimental portions of the research and the contributions of J.R.E., R.L.S., Z.P., J.K., and J.R.L. were supported by the Center for Gas Separations, an Energy Frontier Research Center supported by the U.S. Department of Energy, Office of Science, Office of Basic Energy Sciences, under Award No. DE-SC0001015. J.R.L. serves as a director of and has a financial interest in Mosaic Materials, Inc., a start-up company working to commercialize metal–organic frameworks of the type investigated here. Some of these materials are the subject of patent applications submitted by the University of California, Berkeley.

DATA AVAILABILITY

All data needed to evaluate the conclusions in this paper are present in this paper. Additional data that support the findings of this study are available from the corresponding author upon reasonable request.

REFERENCES

[1] D. Britt, H. Furukawa, B. Wang, T. G. Glover, and O. M. Yaghi, Proc. Natl. Acad. Sci. U. S. A. **106**, 20637 (2009).
[2] K. Sumida, D. L. Rogow, J. A. Mason, T. M. McDonald, E. D. Bloch, Z. R. Herm, T.-H. Bae, and J. R. Long, Chem. Rev. **112**, 724 (2012).
[3] H. Furukawa, K. E. Cordova, M. O'Keeffe, and O. M. Yaghi, Science **341**, 1230444 (2013).
[4] T. M. McDonald, W. R. Lee, J. A. Mason, B. M. Wiers, C. S. Hong, and J. R. Long, J. Am. Chem. Soc. **134**, 7056 (2012).
[5] T. M. McDonald, J. A. Mason, X. Kong, E. D. Bloch, D. Gygi, A. Dani, V. Crocellà, F. Giordanino, S. O. Odoh, W. S. Drisdell, B. Vlaisavljevich, A. L. Dzubak, R. Poloni, S. K. Schnell, N. Planas, K. Lee, T. Pascal, L. F. Wan, D. Prendergast, J. B. Neaton, B. Smit, J. B. Kortright, L. Gagliardi, S. Bordiga, J. A. Reimer, and J. R. Long, Nature **519**, 303 (2015).
[6] J. A. Mason, T. M. McDonald, T.-H. Bae, J. E. Bachman, K. Sumida, J. J. Dutton, S. S. Kaye, and J. R. Long, J. Am. Chem. Soc. **137**, 4787 (2015).
[7] A. Schneemann, V. Bon, I. Schwedler, I. Senkovska, S. Kaskel, and R. A. Fischer, Chem. Soc. Rev. **43**, 6062 (2014).
[8] E. R. Engel, A. Jouaiti, C. X. Bezuidenhout, M. W. Hosseini, and L. J. Barbour, J. Angew. Chem., Int. Ed. **56**, 8874 (2017).
[9] F.-X. Coudert, M. Jeffroy, A. H. Fuchs, A. Boutin, and C. Mellot-Draznieks, J. Am. Chem. Soc. **130**, 14294 (2008).
[10] C. Triguero, F.-X. Coudert, A. Boutin, A. H. Fuchs, and A. V. Neimark, J. Phys. Chem. Lett. **2**, 2033 (2011).
[11] D. Bousquet, F.-X. Coudert, A. G. J. Fossati, A. V. Neimark, A. H. Fuchs, and A. Boutin, J. Chem. Phys. **138**, 174706 (2013).
[12] A. Ghysels, L. Vanduyfhuys, M. Vandichel, M. Waroquier, V. Van Speybroeck, and B. Smit, J. Phys. Chem. C **117**, 11540 (2013).
[13] C. M. Simon, E. Braun, C. Carraro, and B. Smit, Proc. Natl. Acad. Sci. U. S. A. **114**, E287 (2017).
[14] J. J. Binney, N. J. Dowrick, A. J. Fisher, and M. E. Newman, *The Theory of Critical Phenomena: An Introduction to the Renormalization Group* (Oxford University Press, 1992).
[15] J. Kundu, J. F. Stilck, J.-H. Lee, J. B. Neaton, D. Prendergast, and S. Whitelam, Phys. Rev. Lett. **121**, 015701 (2018).
[16] R. Evans, J. Phys.: Condens. Matter **2**, 8989 (1990).
[17] P. A. Monson, Microporous Mesoporous Mater. **160**, 47 (2012).
[18] S. B. Smith, Y. Cui, and C. Bustamante, Science **271**, 795 (1996).
[19] S. Cocco, J. Yan, J.-F. Léger, D. Chatenay, and J. F. Marko, Phys. Rev. E **70**, 011910 (2004).
[20] S. Whitelam, S. Pronk, and P. L. Geissler, BioPhys. J. **94**, 2452 (2008).
[21] H. Fu, H. Chen, J. F. Marko, and J. Yan, Nucleic Acids Res. **38**, 5594 (2010).
[22] R. L. Siegelman, T. M. McDonald, M. I. Gonzalez, J. D. Martell, P. J. Milner, J. A. Mason, A. H. Berger, A. S. Bhown, and J. R. Long, J. Am. Chem. Soc. **139**, 10526 (2017).

Published under license by AIP Publishing

[23]D. T. Gillespie, J. Phys. Chem. **81**, 2340 (1977).
[24]Such curves are often referred to as "isobars," even though the system is not in equilibrium. The true equilibrium isobar has a unique value as a function of temperature.
[25]D. Wilms, A. Winkler, P. Virnau, and K. Binder, Phys. Rev. Lett. **105**, 045701 (2010).
[26]P. G. Debenedetti, *Metastable Liquids: Concepts and Principles* (Princeton University Press, 1996).
[27]D. H. Everett and W. I. Whitton, Trans. Faraday Soc. **48**, 749 (1952).
[28]D. Everett, Trans. Faraday Soc. **50**, 1077 (1954).
[29]M. Kruk, M. Jaroniec, and A. Sayari, Adsorption **6**, 47 (2000).
[30]M. McNall, R. L. Laurence, and W. Curtis Conner, Microporous Mesoporous Mater. **44-45**, 709 (2001).
[31]G. A. Tompsett, L. Krogh, D. W. Griffin, and W. C. Conner, Langmuir **21**, 8214 (2005).
[32]P. I. Ravikovitch and A. V. Neimark, Adsorption **11**, 265 (2005).
[33]A. C. Forse, M. I. Gonzalez, R. L. Siegelman, V. J. Witherspoon, S. Jawahery, R. Mercado, P. J. Milner, J. D. Martell, B. Smit, B. Blümich *et al.*, J. Am. Chem. Soc. **140**, 1663 (2018).
[34]U. Seifert, Phys. Rev. Lett. **95**, 040602 (2005).

Published under license by AIP Publishing